Article

Effect of External Electric Fields on the C–H Bond Activation Reactivity of Nonheme Iron–Oxo Reagents

Hajime Hirao, Hui Chen, Maria Angels Carvajal, Yong Wang, and Sason Shaik

J. Am. Chem. Soc., **2008**, 130 (11), 3319-3327 • DOI: 10.1021/ja070903t

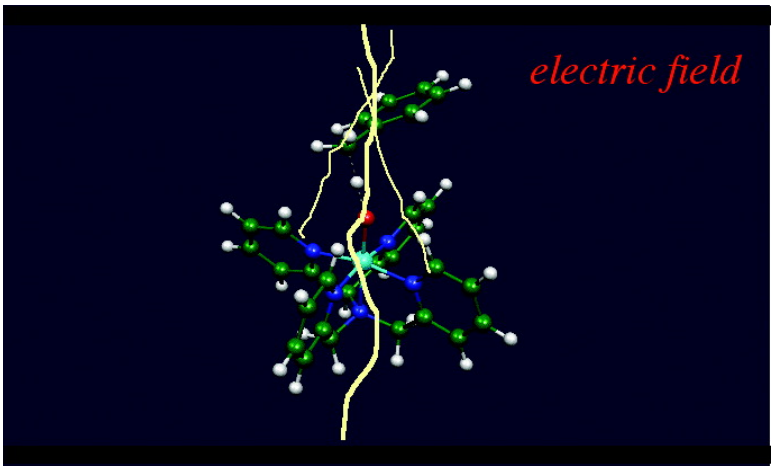

More About This Article

Additional resources and features associated with this article are available within the HTML version:

- Supporting Information
- Access to high resolution figures
- Links to articles and content related to this article
- Copyright permission to reproduce figures and/or text from this article

View the Full Text HTML

J|A|C|S
ARTICLES
Published on Web 02/26/2008

Effect of External Electric Fields on the C−H Bond Activation Reactivity of Nonheme Iron−Oxo Reagents

Hajime Hirao, Hui Chen, Maria Angels Carvajal, Yong Wang, and Sason Shaik*

The Institute of Chemistry and the Lise Meitner-Minerva Center for Computational Quantum Chemistry, The Hebrew University of Jerusalem, 91904 Jerusalem, Israel

Received February 8, 2007; E-mail: sason@yfaat.ch.huji.ac.il

Abstract: The effect of external electric fields (EFs) on the reactivity of nonheme iron(IV)−oxo species toward alkanes is investigated computationally using density functional theory. It is shown that an external EF changes the energy landscape of the process and thereby impacts the mechanisms, rates, and selectivities of the reactions, in a manner dependent on the nature of the iron(IV)−oxo/alkane pair. When the iron−oxo species is a good electron acceptor, like N4PyFeO^{2+}, and the alkane is a good electron donor, like toluene, the application of the EF changes the mechanism from hydrogen abstraction to electron transfer. With cyclohexane, which is a poorer electron donor than toluene, the EF promotes hydride transfer and generates a carbocation. However, in the reaction between a poorer electron acceptor TMC(SR)FeO^{+} and cyclohexane, the EF preserves the hydrogen abstraction/rebound mechanism but improves its features by lowering the barriers for both the C−H activation and rebound steps; larger effects were observed for the quintet-state reaction. In all cases, the EF effect obeys a selection rule; the largest effects are observed when the EF vector is aligned with the Fe═O axis (*z*) and directed along the molecular dipole. As such, *an EF aligned in the direction of the electron flow from substrate to the iron−oxo center lowers the reaction barrier and affects both the reactivity and selectivity of the molecular catalysts*.

1. Introduction

External electric fields (EFs) can affect a variety of chemical events including electron-transfer reactions,[1−3] charge transfer between surfaces,[4] small-molecule−surface interactions,[5,6] and electron transport in molecular devices,[7−9] and they can also induce conformational changes and isomerization processes.[10−13] There has been growing interest in the use of external EFs to modulate chemical reactions that involve bond-forming and bond-breaking steps.[14−18] Recently, the Jerusalem group[14] showed that EFs aligned along the Fe−O bond of compound I (Cpd I) of cytochrome P450 change the potential energy surface and can be used to control the chemoselectivity of propene oxidation: simply reversing the EF direction along the Fe═O bond leads either to selective C−H activation or to C═C activation. Here we demonstrate new features of EF effect on chemical reactivity in the C−H activation reactions by synthetic nonheme iron−oxo reagents, such as the ones shown in Scheme 1.[19] As shall be seen, depending on the iron−oxo reagent and the organic molecule, the application of EFs can change the mechanism, generate new reaction intermediates, and most importantly, *EFs will regulate the stereospecificity and rate of a C−H bond activation reaction by a synthetic nonheme iron−oxo reagent*.

Reagents like N4PyFe^{IV}O^{2+} (**K$_{N4Py}$**) or TMC(SR)Fe^{IV}O^{+} (**K$_{TMC(SR)}$**) (Scheme 1) are known to perform hydrogen abstraction (H-abstraction) reactions; **K$_{N4Py}$** can activate even strong C−H bonds like those in cyclohexane (**CH**) or toluene (**TE**),

(1) (a) Franzen, S.; Goldstein, R. F.; Boxer, S. G. *J. Phys. Chem.* **1990**, *94*, 5135−5149. (b) Franzen, S.; Lao, K.; Boxer, S. G. *Chem. Phys. Lett.* **1992**, *197*, 380−388. (c) Franzen, S.; Boxer, S. G. *J. Phys. Chem.* **1993**, *97*, 6304−6318. (d) Lao, K.; Franzen, S.; Stanley, R. J.; Lambright, D. G.; Boxer, S. G. *J. Phys. Chem.* **1993**, *97*, 13165−13171. (e) Lao, K.; Franzen, S.; Steffen, M.; Lambright, D.; Stanley, R.; Boxer, S. G. *Chem. Phys.* **1995**, *197*, 259−275. (f) Zhou, H.; Boxer, S. G. *J. Phys. Chem. B* **1998**, *102*, 9139−9147. (g) Treynor, T. P.; Boxer, S. G. *J. Phys. Chem. A* **2004**, *108*, 1764−1778.
(2) Murgida, D. H.; Hildebrandt, P. *Acc. Chem. Res.* **2004**, *37*, 854−861.
(3) Seki, K.; Traytak, S. D.; Tachiya, M. *J. Chem. Phys.* **2003**, *118*, 669−679.
(4) Tóbik, J.; Dal Corso, A.; Scandolo, S.; Tosatti, E. *Surf. Sci.* **2004**, *566*−*568*, 644−649.
(5) Leung, K.; Rempe, S. B.; Schultz, P. A.; Sproviero, E. M.; Batista, V. S.; Chandross, M. E.; Medforth, C. J. *J. Am. Chem. Soc.* **2006**, *128*, 3659−3668.
(6) Harikumar, K. R.; Polanyi, J. C.; Sloan, P. A.; Ayissi, S.; Hofer, W. A. *J. Am. Chem. Soc.* **2006**, *128*, 16791−16797.
(7) (a) Reed, M. A.; Zhou, C.; Muller, C. J.; Burgin, T. P.; Tour, J. M. *Science* **1997**, *278*, 252−254. (b) Chen, J.; Reed, M. A.; Rawlett, A. M.; Tour, J. M. *Science* **1999**, *286*, 1550−1552. (c) Blum, A. S.; Kushmerick, J. G.; Long, D. P.; Patterson, C. H.; Yang, J. C.; Henderson, J. C.; Yao, Y.; Tour, J. M.; Shashidhar, R.; Ratna, B. R. *Nat. Mater.* **2005**, *4*, 167−172.
(8) Troisi, A.; Ratner, M. A. *J. Am. Chem. Soc.* **2002**, *124*, 14528−14529.
(9) Li, Y.; Zhao, J.; Yin, X.; Yin, G. *J. Phys. Chem. A* **2006**, *110*, 11130−11135.
(10) Masunov, A.; Dannenberg, J. J.; Contreras, R. H. *J. Phys. Chem. A* **2001**, *105*, 4737−4740.
(11) Alemani, M.; Peters, M. V.; Hecht, S.; Rieder, K.-H.; Moresco, F.; Grill, L. *J. Am. Chem. Soc.* **2006**, *128*, 14446−14447.
(12) Choi, Y. C.; Pak, C.; Kim, K. S. *J. Chem. Phys.* **2006**, *124*, 094308/1-094308/4.
(13) Karafiloglou, P. *J. Comput. Chem.* **2006**, *27*, 1883−1891.
(14) Shaik, S.; de Visser, S. P.; Kumar, D. *J. Am. Chem. Soc.* **2004**, *126*, 11746−11749.
(15) Giuseppone, N.; Lehn, J.-M. *Angew. Chem., Int. Ed.* **2006**, *45*, 4619−4624.
(16) Harada, A.; Kataoka, K. *J. Am. Chem. Soc.* **2003**, *125*, 15306−15307.
(17) Virányi, Z.; Szommer, A.; Tóth, Á.; Horváth, D. *Phys. Chem. Chem. Phys.* **2004**, *6*, 3396−3401.
(18) De Biase, P. M.; Doctorovich, F.; Murgida, D. H.; Estrin, D. A. *Chem. Phys. Lett.* **2007**, *434*, 121−126.
(19) (a) Kaizer, J.; Klinker, E. J.; Oh, N. Y.; Rohde, J.-U.; Song, W. J.; Stubna, A.; Kim, J.; Münck, E.; Nam, W.; Que, L., Jr. *J. Am. Chem. Soc.* **2004**, *126*, 472−473. (b) Bukowski, M. R.; Koehntop, K. D.; Stubna, A.; Bominaar, E. L.; Halfen, J. A.; Münck, E.; Nam, W.; Que, L., Jr. *Science* **2005**, *310*, 1000−1002.

Scheme 1. (a) Multidentate Ligands (N4Py, TMC(SR)), (b) the Corresponding Iron−Oxo Complexes ($\mathbf{K_L}$) Their Potential Reactions with Alkanes (R−H), and (c) the Alkanes Used in the Study (**CH**, **TE**)

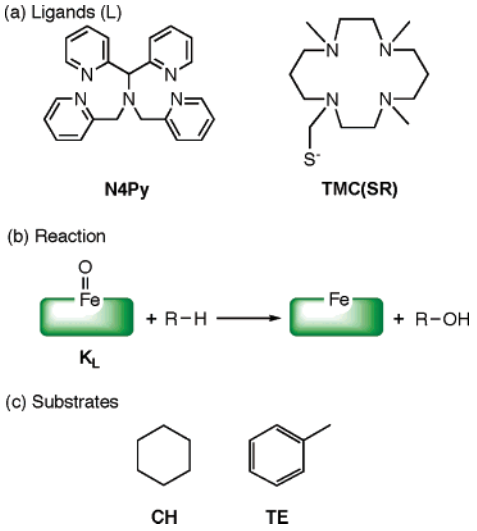

albeit sluggishly,[19a] while $\mathbf{K_{TMC(SR)}}$ can react only with weak C−H bonds like those in 9,10-dihydroanthracene, but in this case, instead of the corresponding alcohol the final product is anthracene.[19b] DFT calculations show that the mechanism has additional important features; it involves the two closely lying spin-states of $^{2S+1}\mathbf{K_L}$, a ground triplet state ($S = 1$) and a low-lying quintet excited state ($S = 2$).[20] Thus, as exemplified in Figure 1, the reaction of $^{3,5}\mathbf{K_{N4Py}}$ with **TE**[20] proceeds by a

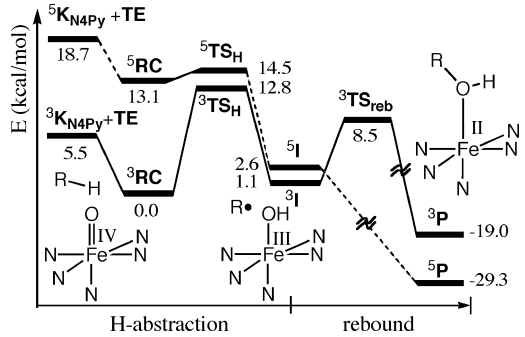

Figure 1. B3LYP/LACVP gas-phase energy profiles for the reaction of $\mathbf{K_{N4Py}}$ with toluene (**TE**) in the two spin states.[20] **TE** is denoted as R−H.

rebound mechanism, involving initial H-abstraction, followed by rebound of the radical to form the ferric−alcohol product complexes, $^{3,5}\mathbf{P}$. The reaction starts on the triplet ground state. However, the triplet−quintet energy gap shrinks in the H-abstraction step, the two states get close in energy at the intermediate stage, and subsequently, the energy profiles bifurcate. The triplet state rebound faces a significant barrier, via $^{3}\mathbf{TS_{reb}}$, while on the quintet state the rebound is barrier free. Thus, theory predicts that a reaction of the iron−oxo reagent may involve a mixture of quintet and triplet pathways, the latter resulting in a significant loss of stereoselectivity of stereochemically labeled R−H substrates and generation of byproducts typical of steps involving radicals. More extended basis sets change the relative energies of the two spin sates but do not affect this general conclusion.[20] Additionally, since $\mathbf{K_{N4Py}}$ is

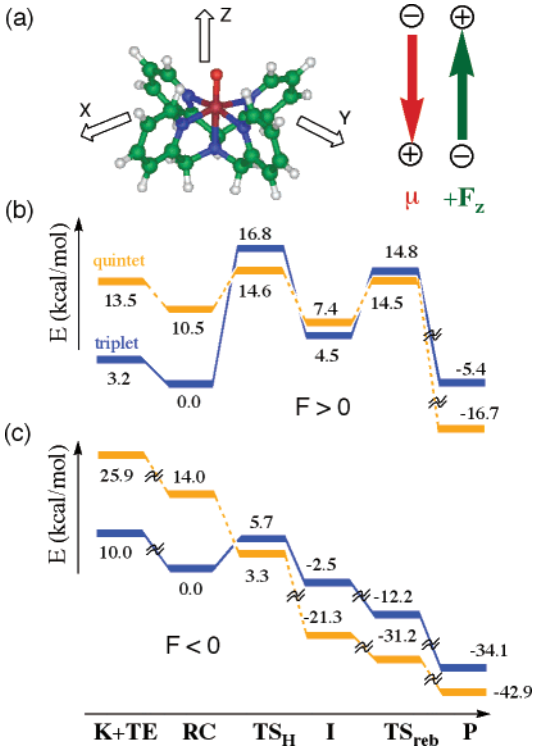

Figure 2. (a) Reagent, the + directions of the electric field (F_z) and dipole moment (μ), and B3LYP/LACVP reaction energy profiles under the EFs oriented along the *z*-axis: (b) $F_z = +0.0075$ au; (c) $F_z = -0.0075$ au.

positively charged ($z = 2+$), the barriers in a solvent are higher than the gas-phase values in Figure 1, which is true for other reagents of this family, as well.[20] Therefore, the iron−oxo reagent is expected to be a moderately sluggish bond activator that also leads to nonstereoselective results and a variety of side reactions. A major goal of this paper is to demonstrate that the application of EFs on the reactions of the iron−oxo reagents, $\mathbf{K_{N4Py}}$ and $\mathbf{K_{TMC(SR)}}$, in Scheme 1 with **TE** and **CH** can drastically affect the mechanism of these reactions and even improve the stereospecificity and the reaction rate by selective interaction with the two spin states.

2. Computational Methods

Calculations were performed using the B3LYP[21] DFT method with the double-ζ LACVP[22] basis set under the influence of EF of a variety of strengths: −0.0125, −0.0075, −0.0050, −0.0025, +0.0025, +0.0050, +0.0075, and +0.0125 au (1 au = 51.4 V/Å). All calculations were carried out with Gaussian 03[23] using the "Field=M ± N" keyword, which defines the EF axis and its direction and magnitude. Changes were observed for the EFs along the three axes *x*, *y*, *z*, where *z* is oriented along the Fe=O bond of the $\mathbf{K_L}$ reagent and *x*, *y* lie in the demiplane defined by the nitrogenous ligand (see Figure 2a). For the reasons discussed later, the calculations of $\mathbf{K_{TMC(SR)}}$ were limited to an EF of −0.0075 au along the *z*-axis.

Initially, the EF effects were estimated by single point calculations on the gas-phase optimized critical points in the reaction of $^{3,5}\mathbf{K_{N4Py}}$ with **TE**. Subsequently, we optimized the critical structures in the

(20) Hirao, H.; Kumar, D.; Que, L., Jr.; Shaik, S. *J. Am. Chem. Soc.* **2006**, *128*, 8590−8606.

(21) (a) Becke, A. D. *J. Chem. Phys.* **1992**, *96*, 2155−2160. (b) Becke, A. D. *J. Chem. Phys.* **1992**, *97*, 9173−9177. (c) Becke, A. D. *J. Chem. Phys.* **1993**, *98*, 5648−5652. (d) Lee, C.; Yang, W.; Parr, R. G. *Phys. Rev. B* **1988**, *37*, 785−789.

(22) The LACVP series is derived from LANL2DZ; see the following: (a) Hay, J. P.; Wadt, W. R. *J. Chem. Phys.* **1985**, *82*, 299−310. (b) Friesner, R. A.; Murphy, R. B.; Beachy, M. D.; Ringnalda, M. N.; Pollard, W. T.; Dunietz, B. D.; Cao, Y. *J. Phys. Chem. A* **1999**, *103*, 1913−1928.

(23) Frisch, M. J.; et al. *Gaussian 03*; Gaussian, Inc.: Wallingford, CT, 2004.

presence of the EF for all the reactions of the two iron−oxo reagents with the two substrates, **TE** and **CH**. All data are collected in the Supporting Information (SI), while the key results are discussed here.

3. Results and Discussion

3.1. Reaction of K_{N4Py} with TE: Single Point Energy Correction Due to EF Effects. Figure 2a shows the K_{N4Py} reagent in the coordinate axes system and defines the positive direction of the field vis-à-vis the axis and the direction of the molecular dipole moment, μ. Figure 2b,c shows the energy profiles obtained by single point calculations on the critical species in Figure 1 in the presence of EFs. The energetic effects of the EF oriented along the *x* and *y* directions were found to be comparatively smaller, albeit not negligible, and the corresponding data were relegated to the SI document. By contrast, orientation of the EF along the *z* direction (F_z) changed the energy landscape of the reaction in a major way. This was the case for any field strength used (see SI, Figures S1 and S2). As such, Figure 2b,c and all subsequent ones focus on the impact of F_z only.

Thus, application of the EF in the $+z$ direction (Figure 2b) increased all the barriers compared with the field-free reaction (Figure 1). Moreover, the quintet surface now crosses the triplet state and develops a rebound barrier.[24] Therefore, an EF in the $+z$ direction appears to diminish the reactivity of $^3K_{N4Py}$ and transform the quintet process to a stepwise one. By contrast, flipping the EF orientation to the $-z$ direction lowered the barrier to H-abstraction on the triplet surface and eliminated the rebound barrier (Figure 2c). The quintet surface became barrier free all the way down to the alcohol complex.

3.2. Reaction of K_{N4Py} with TE: Effects of Geometry Optimization in the Presence of EF. The above single-point calculations show that the reactivity can be significantly affected by external EFs, which change the energy landscape of the reaction. However, the EFs alter also the atomic forces and consequently the structure of each stationary point is expected to undergo a change compared with the bare reaction in the absence of an external EF. To test the impact of geometry changes, we carried out geometry optimizations of a few key species, K_{N4Py}, **RC**, and **I**, in the presence of an EF of −0.0075 au, which was demonstrated above in Figure 2 to enhance the reactivity in the single-point calculations. The calculations show that the iron−oxo reagent K_{N4Py} remains intact in the EF and its geometry does not change to any appreciable extent. However, geometry optimization of the reactant complex, **RC**, and of the iron−hydroxo/radical complex, **I**, under the influence of $F_z = -0.0075$ au, changed the nature of the species, as summarized in Scheme 2.

Thus, upon geometry optimization of the quintet reactant complex, ^{5}**RC**, electron transfer occurred spontaneously from **TE** to K_{N4Py}, and the resultant radical cation $TE^{+\bullet}$ flew away from the iron−oxo unit, since the charge-separated state is more stable under the EF influence (Scheme 2a). Similarly, when the iron−hydroxo/R$^\bullet$ complex ^{5}**I** was subjected to $F_z = -0.0075$ au, the radical transferred one electron to the iron−hydroxo complex and generated a carbocation, R^+, that flew away from the substrate (Scheme 2b). ^{3}**RC** remained intact, while ET occurred in ^{3}**I**, as shown in Scheme 2b. This means that even though the reaction (Figure 2) starts with ^{3}**RC**, since it crosses over to the quintet intermediate, ^{5}**I**, it will produce a benzylic carbocation, which is likely to exhibit reactivity different from that of the corresponding radical. When the substrate (RH) is a more powerful electron donor than toluene, one would expect that already at the ground state, ^{3}**RC**, the EF will induce ET and will generate a radical cation, $RH^{+\bullet}$. With **CH**, which is a poorer electron donor than **TE**, ET again occurred in the geometry optimizations of ^{5}**RC** and ^{5}**I**. However, no electron transfer was observed either in ^{3}**RC** or in ^{3}**I**. These results indicate that *the application of the EF on the reactions of the iron−oxo reagent K_{N4Py}* with alkanes *can change the reaction mechanism from H-abstraction to electron transfer (ET)*, when the alkane is a good electron donor and/or generate a new reaction intermediate, carbocation, R^+ instead of a radical R$^\bullet$, or when the alkane is a poor electron donor and the EF is relatively weak (i.e., <0.0075 au).

Scheme 2. Representation of the Mechanistic Changes Due to the Application of a External EF on the (a) ^{5}**RC** and (b) ^{5,3}**I** Species[a]

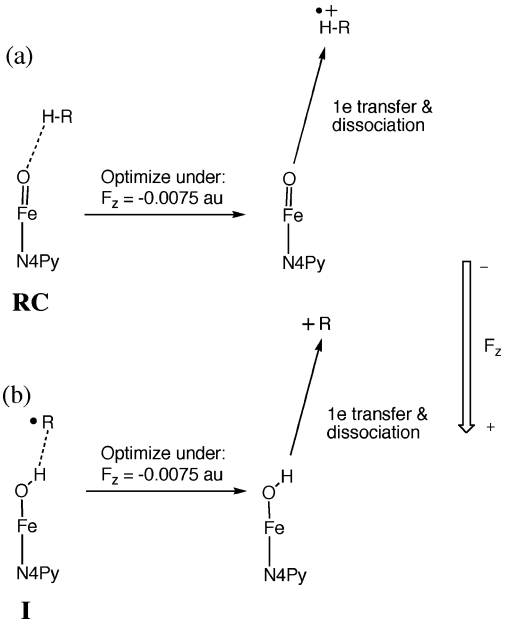

[a]The field vector is shown as F_z and points in the $-z$ direction.

3.3. Reaction of $K_{TMC(SR)}$ with CH. The reactions of K_{N4Py} are prone to ET or to generation of carbocations, since this reagent is doubly charged and its gas-phase electron affinity is very large (182.8 kcal/mol). Therefore, to study the effect of EFs on H-abstraction reactivity, we turned to $K_{TMC(SR)}$ which is only singly positive and has a much smaller gas-phase electron affinity also due to the electron-releasing effect of the thiolate ligand (119.5 kcal/mol). This reagent was coupled to **CH**, which is a rather poor electron donor. Our reasoning is that this reactant pair would maintain the H-abstraction and then hopefully also rebound to give an alcohol, as seen in Scheme 3, even in the presence of the external EF.

3.3.1. Reaction of $K_{TMC(SR)}$ with CH in the Absence and Presence of External EF. Since the single-point calculations in Figure 2 showed that a positive EF raises the H-abstraction barriers, we carried out the calculations only for the negatively oriented field, using $F_z = -0.0075$ au. Figure 3 shows the energy profiles for the reaction between $^{3,5}K_{TMC(SR)}$ and **CH**. Without an EF (Figure 3a), the H-abstraction barrier in the triplet

(24) $^5TS_{reb}$ (Figure 2) represents a single-point calculation with EFs of a structure along a rebound scan at *r*(C−O) distance = 2.5 Å. This structure was used because $^5TS_{reb}$ was not obtained in the gas phase. See Figure S14.

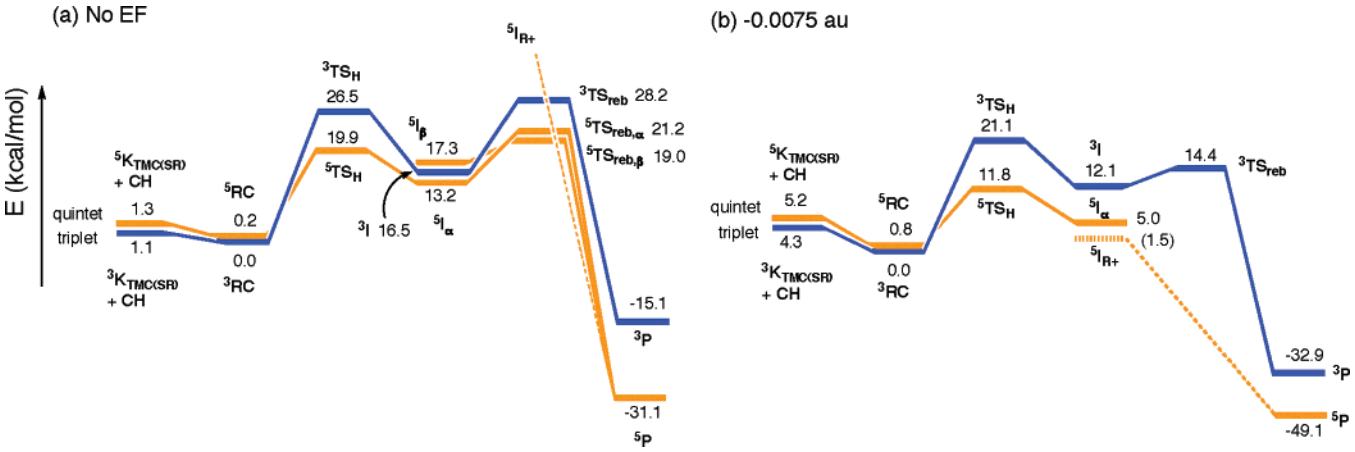

Figure 3. Energy profiles for the reaction between $\mathbf{K_{TMC(SR)}}$ and **CH** at the B3LYP/LACVP level. The various intermediate states are described in the text: (a) profiles in the absence of EF; (b) profiles in the presence of EF, $F_z = -0.0075$ au. The relative energy of $^5\mathbf{I_{R^+}}$ is taken from an energy scan at r(C−O) = 3.0 Å (Figure S15B).

Scheme 3. Postulated Reaction in the Presence of EF between $\mathbf{K_{TMC(SR)}}$ and **CH**, Consisting of H-Abstraction Followed by Radical Rebound

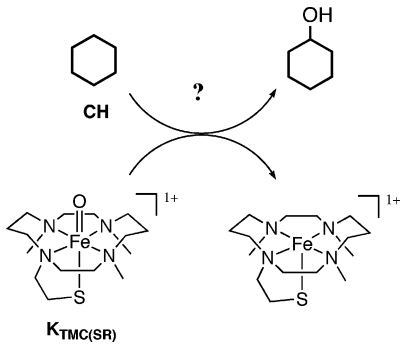

state is as high as 26.5 kcal/mol. The rebound barrier is even higher (the TS lies at 28.2 kcal/mol), and therefore, the rate-controlling step on the triplet surface should be the rebound step; with such a high barrier the radical is likely to generate a variety of byproducts.

While the quintet transition state,$^5\mathbf{TS_H}$, in Figure 3a, is lower in energy than $^3\mathbf{TS_H}$, still, the quintet barrier is too high (19.7 kcal/mol) to cause an efficient bond activation reaction. These triplet/quintet barriers are much higher than those for the reaction between $\mathbf{K_{N4Py}}$ and **TE**, i.e., 12.8/1.4 kcal/mol (Figure 1), respectively. Indeed, experimentally, $\mathbf{K_{TMC(SR)}}$ is known to be a much more sluggish oxidant than $\mathbf{K_{N4Py}}$.[19] However, as seen in Figure 3b, under the influence of an external EF, oriented opposite to the FeO direction, these H-abstraction barriers are lowered significantly, for both spin states, but the energy lowering is more significant in the quintet state where the barrier is now only 11.0 kcal/mol. These energy lowering effects of the two H-abstraction barriers as well as the larger effect on the quintet barrier are very similar to the effect observed in the single-point calculations in the presence of an EF, above in Figure 2.

Let us turn now to the effect of the EF on the rebound step in Figure 3, part a vs part b. In the absence of an external EF the triplet rebound barrier is seen to be as large as 11.7 kcal/mol (Figure 3a). When the EF is turned on, the barrier is dramatically lowered to 2.3 kcal/mol (Figure 3b). Therefore, the triplet state surface is transformed also qualitatively, and in the presence of an EF of $F_z = -0.0075$ au, the rate-controlling step is now H-abstraction, while the rebound step is predicted to become very fast. *As such, the application of the EF is predicted to enhance the triplet reaction and minimize the generation of byproducts.*

The quintet rebound step shown in Figure 3 is somewhat more complex. There exist a few possible species for the quintet manifold of the intermediate species **I**. The electronic structures for the three key species are shown in Scheme 4.

The lowest quintet intermediate is a hexaradicaloid species, $^5\mathbf{I}_\alpha$, which involves an iron−hydroxo/radical intermediate, TMC(SR)$Fe^{III}OH^+$/•R.[20] This species has five unpaired electrons in the d-block orbital of iron−hydroxo ($\delta^1\pi^*_{xz}{}^1\pi^*_{yz}{}^1\sigma^*_{xy}{}^1\sigma^*_{z^2}{}^1$) and one in the ϕ_C orbital of the cyclohexyl radical (note that $\sigma^*_{z^2}$ and ϕ_C constitute an antiferromagentic orbital pair). A higher radical complex state is indicated as $^5\mathbf{I}_\beta$ and involves the $\delta^2\pi^*_{xz}{}^1\pi^*_{yz}{}^1\sigma^*_{xy}{}^1\ \phi_C{}^1$ configuration. The subscripts α and β in these two local minima species *denote the directions of the spin shifted from substrate to the iron center in the H-abstraction step* (Scheme 4). Still higher is the quintet state that correlates down to products and is labeled in Scheme 4 as $^5\mathbf{I_{R^+}}$ (Figure S15C). The latter species involves a cyclohexyl carbocation and four unpaired electrons on the iron−hydroxo moiety in a $\delta^2\pi^*_{xz}{}^1\pi^*_{yz}{}^1\sigma^*_{xy}{}^1\sigma^*_{z^2}{}^1$ configuration, hence TMC(SR)$Fe^{II}OH/R^+$. $^5\mathbf{I_{R^+}}$ could be calculated here (e.g., Figure 3a) at long C−O distances using a backward scan starting from $^5\mathbf{P}$; however, the $^5\mathbf{I_{R^+}}$ species was not a local minimum. These states can in principle exist also for the reaction of $\mathbf{K_{N4Py}}$ in Figure 1; however, in the reaction of $\mathbf{K_{N4Py}}$ the $^5\mathbf{I}_\beta$ state was not a local minimum and it internally, smoothly, and barrierlessly transformed to the product state ($^5\mathbf{P}$).[20] On the basis of recent models for the rebound process,[25,26] we recall that, in the rebound step from $^5\mathbf{I}_\alpha$ to $^5\mathbf{P}$, an electron shifts from the substrate orbital to the δ orbital, and what accounts for the difference between $\mathbf{K_{N4Py}}$ and $\mathbf{K_{TMC(SR)}}$ is that the former is a much better electron acceptor than the latter due to the electron-releasing power of the thiolate ligand. Thus, in the reaction of $\mathbf{K_{N4Py}}$ with **TE**,[20] no rebound barrier was obtained on the quintet surface (see Figure S13b). In contrast, for the poorer electron acceptor, $\mathbf{K_{TMC(SR)}}$, the rebound barriers are significant even in the quintet states (8.0 kcal/mol from $^5\mathbf{I}_\alpha$ to $^5\mathbf{TS_{reb,\alpha}}$ and 1.7 kcal/mol from

(25) Shaik, S.; Cohen, S.; de Visser, S. P.; Sharma, P. K.; Kumar, D.; Kozuch, S.; Ogliaro, F.; Danovich, D. *Eur. J. Inorg. Chem.* **2004**, 207−226.
(26) Shaik, S.; Hirao, H.; Kumar, D. *Nat. Prod. Rep.* **2007**, *24*, 533−552.

Scheme 4. Electronic Structure of the Radical Quintet States, TMC(SR)Fe^{III}OH/R•, in the Intermediate Geometry

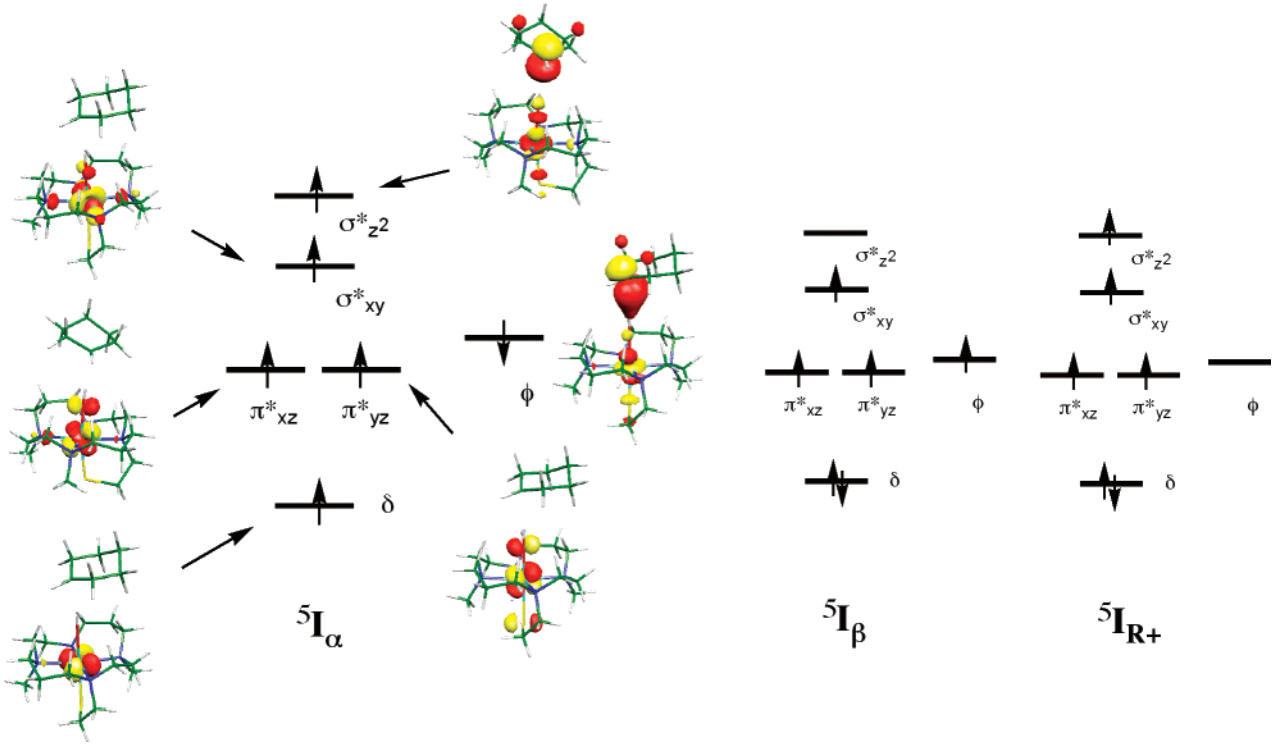

$^5\mathbf{I}_\beta$ to $^5\mathbf{TS}_{\mathbf{reb},\beta}$; see Figure 3a). We note that de Visser[27] found a considerable barrier for the quintet state in the C−H hydroxylation of propene by $\mathbf{K}_{\mathbf{TMC(SR)}}$, compared with a tiny one when the axial ligand of iron was imidazole. The rebound barriers on both the triplet and quintet surfaces in the $\mathbf{K}_{\mathbf{TMC(SR)}}$ reaction may be the root cause of the observation by Que et al.[19b] that the product of the reaction is TMC(SR)Fe^{III} rather than the ferrous complex. Such high rebound barriers will endow the radical with a sufficient lifetime to undergo H-abstraction by another molecule of iron−oxo rather than rebound to give a ferrous−alcohol complex.

The application of the external EF in Figure 3b stabilizes the intermediate states. As the analysis of the reactivity of $\mathbf{K}_{\mathbf{N4Py}}$ revealed, the EF in the $-z$ direction facilitates the electron shift from substrate to the iron center. For this reason, when an EF was applied to $^5\mathbf{I}_\beta$, the unpaired electron in the substrate moiety dropped to the $\sigma^*_{z^2}$ orbital to generate $^5\mathbf{I}_\mathbf{R}^+$ (Figure S15C). Although $^5\mathbf{I}_\mathbf{R}^+$ was not a local minimum, the energy of $^5\mathbf{I}_\mathbf{R}^+$ at r(C−O) = 3.0 Å was found to be 3.5 kcal/mol lower than $^5\mathbf{I}_\alpha$ in the EF (Figures 3 and S15B). It was also found that the $^5\mathbf{I}_\mathbf{R}^+$ species is connected to $^5\mathbf{P}$ without a rebound barrier (dashed lines in Figure 3a,b). *This cationic path is significantly stabilized in the presence of EF*.[28] We could not find a path that connects $^5\mathbf{I}_\alpha$ and $^5\mathbf{P}$ smoothly in the presence of the EF (Figure S15B), presumably due to the single determinant representation of the wave function in the DFT model.[29] Nevertheless, with such a small energy difference between $^5\mathbf{I}_\alpha$ and $^5\mathbf{I}_\mathbf{R}^+$ seen in Figure 3b, we suspect that the transition from $^5\mathbf{I}_\alpha$ to the stable $^5\mathbf{I}_\mathbf{R}^+$ is rather facile in the EF and that the rebound step in the quintet state proceeds favorably without a barrier on the cationic pathway.

In summary, the external EF oriented along the reaction axis (in the negative direction of the z-axis) is shown to lower the barriers for both H-abstraction and radical rebound steps and is thereby expected to both enhance the reaction and minimize the amounts of side products which may result from a long-lived radical species. Unlike the field-free reaction that proceeds only through the hydrogen abstraction reaction,[19b] in the presence of EF one is likely to see the alcohol product. The EF exerts a larger influence on the quintet spin state reaction, even though the effect on the triplet state is also very significant.

3.3.2. Geometries of Species in the Reaction of $\mathbf{K}_{\mathbf{TMC(SR)}}$ with CH in the Absence and Presence of External EF. The optimized geometric features of the species that occur along the H-abstraction step are shown in Figure 4, in the absence ($F_z = 0$) and presence ($F_z = -0.0075$ au) of an external EF. Figure 5 shows the corresponding optimized geometries for the rebound step.

Inspection of Figure 4 reveals that the external EF hardly affects the iron−oxo reagent and slightly loosens the FeO−HC interaction that holds the reactants in the **RC** cluster. A more significant effect is seen in the H-abstraction transition states, $^{3,5}\mathbf{TS}_\mathbf{H}$. Thus, for both spin states, the EF decreases the extents of C−H bond cleavage and O−H bond making in the $\mathbf{TS}_\mathbf{H}$ species, with a more noticeable effect in the quintet state species, $^5\mathbf{TS}_\mathbf{H}$. Consequently, the external EF placed in the direction of the FeO axis shifts both $^5\mathbf{TS}_\mathbf{H}$ and $^3\mathbf{TS}_\mathbf{H}$ to earlier positions along the H-transfer coordinate, more so in the former species. This trend in the geometries of the $\mathbf{TS}_\mathbf{H}$ species is in line with the energy effects on the corresponding H-abstraction

(27) de Visser, S. P. *J. Am. Chem. Soc.* **2006**, *128*, 15809−15818.
(28) Geometry optimization of $^5\mathbf{I}_\beta$ starting from the field-free structure led to separation of the substrate cation after electron transfer ($^5\mathbf{I}_\mathbf{R}^+$) as shown in Scheme 2. However, geometry optimization starting from r(C−O) = 2.8 Å resulted in $^5\mathbf{P}$, and as written in the text, the process connecting $^5\mathbf{I}_\mathbf{R}^+$ to $^5\mathbf{P}$ is barrier free under EF (Figure S15B).
(29) The mixing of the $^5\mathbf{I}_\alpha$ and $^5\mathbf{I}_\mathbf{R}^+$ states is proportional to the overlap of the orbital on the radical, ϕ_C, and the δ orbital on iron. This overlap is very poor, and hence, the mixing is small or negligible (see SI). DFT will not mix these two states. A multiconfigurational treatment may be necessary for the refinement of this detail.

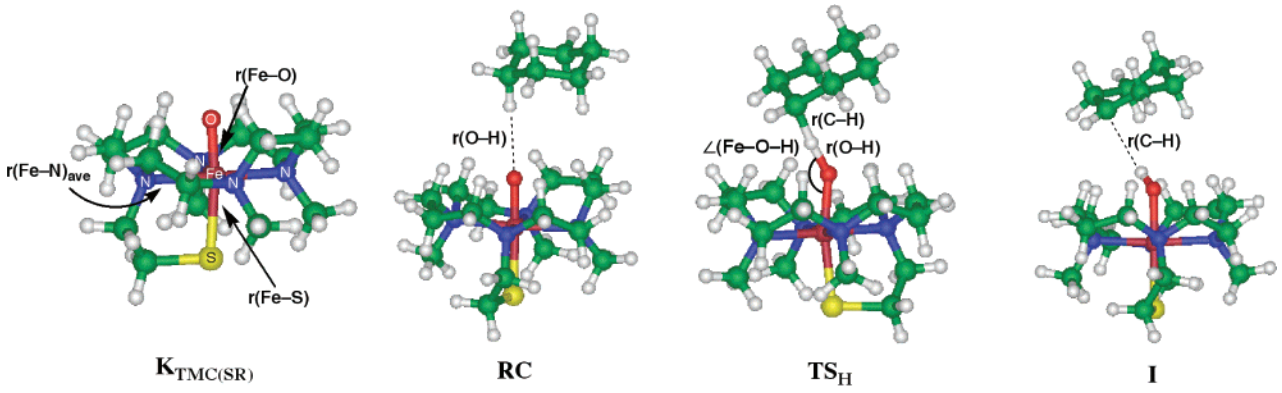

	r(Fe–O)	r(Fe–S)	r(Fe–N)$_{ave}$	r(O---H)	r(C---H)	∠(Fe-O-H)
^{3}K	1.68 (1.67)	2.37 (2.40)	2.14 (2.15)	N/A	N/A	N/A
^{5}K	1.68 (1.67)	2.36 (2.38)	2.23 (2.24)	N/A	N/A	N/A
^{3}RC	1.68 (1.66)	2.37 (2.40)	2.14 (2.15)	2.72 (2.82)	1.10 (1.11)	177.1 (166.0)
^{5}RC	1.69 (1.67)	2.36 (2.38)	2.23 (2.24)	2.70 (2.87)	1.10 (1.11)	171.8 (154.6)
^{3}TS$_H$	1.85 (1.82)	2.36 (2.41)	2.15 (2.15)	1.19 (1.24)	1.39 (1.35)	143.4 (147.6)
^{5}TS$_H$	1.81 (1.79)	2.43 (2.48)	2.25 (2.26)	1.22 (1.32)	1.34 (1.28)	173.6 (174.7)
^{3}I	1.88 (1.85)	2.34 (2.37)	2.15 (2.15)	0.98 (0.99)	2.55 (2.32)	124.7 (129.4)
^{5}I$_\alpha$	1.86 (1.84)	2.43 (2.47)	2.26 (2.27)	0.98 (1.00)	2.18 (2.01)	176.5 (176.4)
^{5}I$_\beta$	1.85 (N/A)	2.34 (N/A)	2.25 (N/A)	0.97 (N/A)	2.42 (N/A)	135.0 (N/A)

Figure 4. Optimized geometries for key structures during the H-abstraction step of the reaction between $\mathbf{K_{TMC(SR)}}$ and cyclohexane without EF (with EF; $F_z = -0.0075$ au). Bond distances are in Å, and bond angles are in degrees

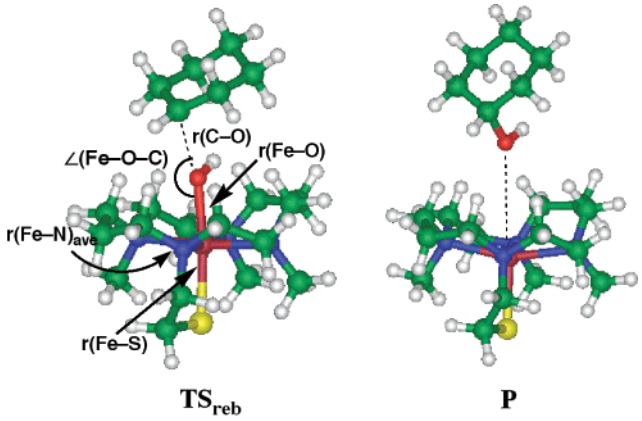

	r(Fe–O)	r(Fe–S)	r(Fe–N)$_{ave}$	r(C---O)	∠(Fe-O-C)
^{3}TS$_{reb}$	2.08 (2.00)	2.40 (2.44)	2.17 (2.19)	2.31 (2.91)	164.1 (169.3)
^{5}TS$_{reb,\alpha}$	2.04 (N/A)	2.43 (N/A)	2.27 (N/A)	2.53 (N/A)	157.1 (N/A)
^{5}TS$_{reb,\beta}$	2.01 (N/A)	2.38 (N/A)	2.25 (N/A)	2.61 (N/A)	169.0 (N/A)
^{3}P	3.88 (3.99)	2.40 (2.45)	2.17 (2.18)	1.49 (1.51)	141.7 (135.6)
^{5}P	4.30 (4.25)	2.37 (2.40)	2.29 (2.29)	1.49 (1.51)	147.8 (143.4)

Figure 5. Optimized geometries for key structures during the rebound step of the reaction between $\mathbf{K_{TMC(SR)}}$ and cyclohexane (with EF; $F_z = -0.0075$ au).

barriers noted above. Thus, driving the transition state to an earlier position along the H-transfer coordinate is expected to lower the barrier.[14,30,31]

Another interesting feature in Figure 4 is the difference between the general orientations of ^{3}**TS$_H$** and ^{5}**TS$_H$**. Inspection of the corresponding FeOH angles shows that the quintet transition state is almost upright and becomes more so when the external EF is turned on. The triplet transition state is more bent, having a significantly smaller FeOH angle of 143.4°, which increases in the presence of the EF to 147.6°. The upright vs bent orientations of these TSs were discussed before[20] and shown to obey orbital selection rules, which will be recalled in the Discussion. The increase of the FeOH angle in both transition states is associated with the stabilization of the species by the EFs, and this is another issue that will be clarified in the Discussion.

The final feature in Figure 4 concerns the geometry of the intermediates ^{3,5}**I**. In both spin states the main effect of the external EFs is seen to be the tightening of the FeOH−C interaction between the iron−hydroxo and the cyclohexyl radical, an effect that accounts for their energy stabilization by the EF. Finally, note the difference in the FeOH angles of the $^5\mathbf{I}_\beta$ and the $^5\mathbf{I}_\alpha$ species: it is almost 180° in the latter species in both the field-free and EF states, while this angle is bent in the field-free state (recall, $^5\mathbf{I}_\beta$ does not exist as a minimum in the presence of the EF).

Inspection of Figure 5 shows that the external EF has a major effect on the triplet rebound transition state, ^{3}**TS$_{reb}$**, which becomes much earlier having a significantly longer C−O and shorter Fe−O bonds compared with the gas-phase species. These geometric changes are in perfect accord with the large barrier lowering effect noted in Figure 3 for the triplet rebound process. There are no corresponding data for the quintet state since the EF renders the rebound process barrier free. Still it is important to note that all the rebound transition states have very large Fe−O−C angles, 157.1−169.3°, and are essentially upright

(30) Shaik, S.; Shurki, A. *Angew. Chem., Int. Ed.* **1999**, *38*, 586−625.
(31) Hammond, G. S. *J. Am. Chem. Soc.* **1955**, *77*, 334−338.

Scheme 5. Schematic Representation of the Effects of EF, Pointing in the Negative Direction of the *z*-Axis, on the Possible Intermediates and Products of the Reactions of $\mathbf{K_{N4Py}}$ with **TE** (Left) and of $\mathbf{K_{TMC(SR)}}$ with **CH** (Right)

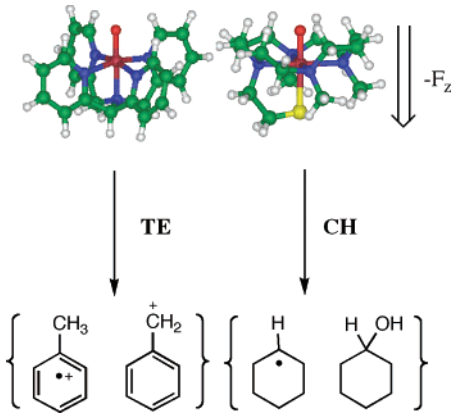

structures under whichever condition they exist as minima (with or without EF).

4. Discussion

As we saw in a previous study,[14] here, too, the effects of external EF on reactivity obey selection rules: (i) The effect is significant in the *z* direction that coincides with the Fe−O bond but less significant in the *x*, *y* directions, in the demiplane of the iron−oxo reagent. (ii) It is adverse when the field points in the +*z* direction ($F_z > 0$) and beneficial when the field is in the −*z* direction ($F_z < 0$), namely in the opposite direction to the Fe═O moiety (see Figure 2).

Scheme 5 summarizes the findings of this study on the effect of EF in the −*z* direction. Thus, using a good electron acceptor iron−oxo reagent, like N4PyFeO^{2+}, and a substrate that is a good electron donor, like toluene, the EF (−*z*) changes the reaction mechanism from C−H bond activation to electron transfer and induces the generation of a carbocation, in this case a benzylic cation. In contrast, when the iron−oxo reagent is a poorer electron acceptor, like TMC(SR)FeO^{+}, and the substrate is a poorer electron donor, like cyclohexane, the EF does not change the reaction type but improves the reactivity and selectivity of the reaction. Thus, the presence of EF lowers the barrier for C−H abstraction and improves the efficiency of the rebound step, on both spin states. Therefore, instead of stopping at the ferric state, TMC(SR)Fe^{III}, as found in the reaction with 9,10-dihydroanthracene,[19b] the EF is expected to transform the energy landscape of the reaction in a manner that enables the formation of alcohol and the ferrous state, TMC(SR)Fe^{II}. Furthermore, the improvement of the rebound step is predicted to minimize byproducts and in the case of stereochemically labeled substrates also to enhance the stereoselectivity of the reaction.

In the space below we attempt to understand these features of the reaction between TMC(SR)FeO^{+} with cyclohexane, which is chemically more interesting than the electron-transfer mechanisms and the carbocation generation found for the reactions of toluene with N4PyFeO^{2+}.

4.1. Origins of Transition State Structures during the Reaction of TMC(SR)FeO^{+} and C_6H_{12}. To facilitate the discussion, we depict in Scheme 6 the evolution of the orbital occupation during the hydroxylation mechanism on the two spin-state surfaces, as established in a recent treatment.[20] It is seen that, during the C−H activation on the triplet state, the H-abstraction step involves an electron shift from the C−H bond orbital (σ_{C-H}) to the π^*_{xz} orbital of the iron−oxo center. Thus,

Scheme 6. Orbital Occupation Evolution Diagram during the Reaction of $\mathbf{K_{TMC(SR)}}$ with Cyclohexane[a]

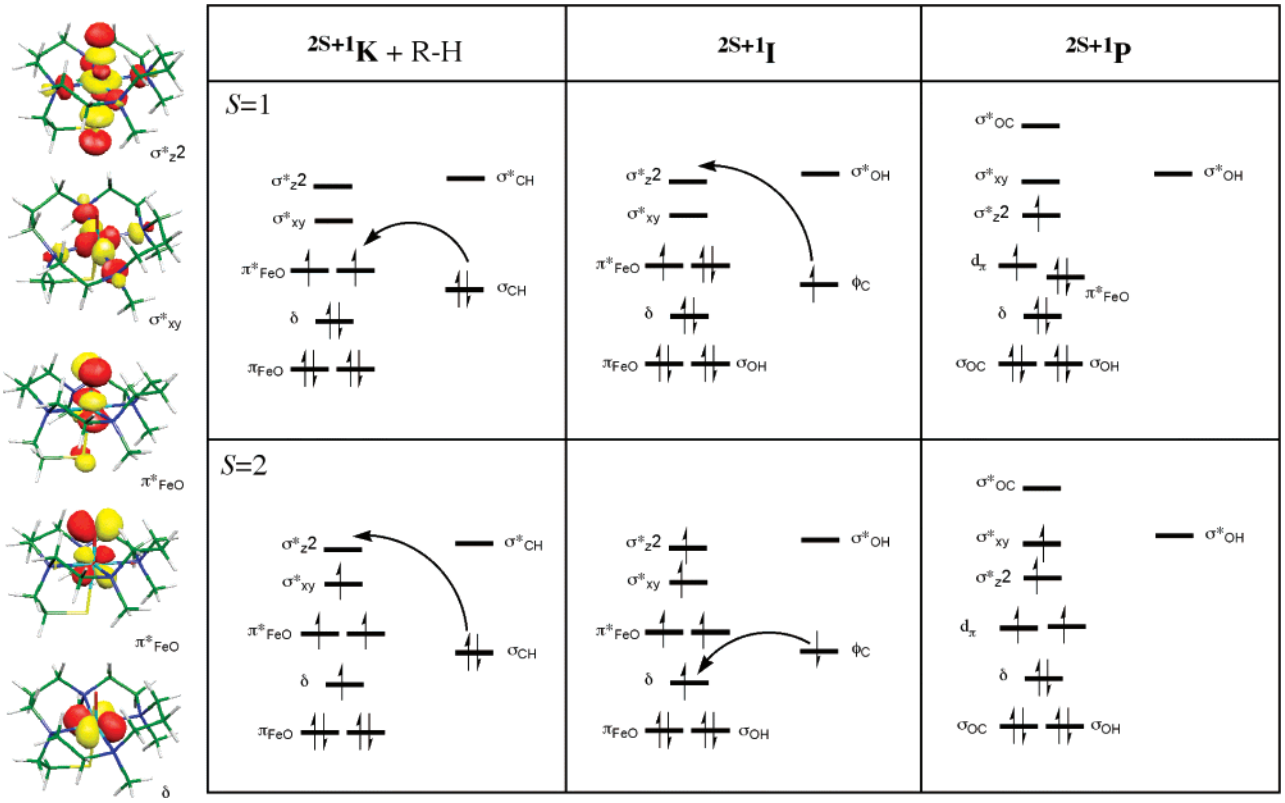

[a] The intermediate shown on the quintet surface is $^5\mathbf{I}_\alpha$. In the $^5\mathbf{I}_\beta$ intermediate (not shown) the electron shifts from ϕ_C to the $\sigma^*_{z^2}$ orbital.

to maximize the overlap between the two orbitals that participate in the electron shift, the transition state species, ^{3}**TS$_H$**, assumes a sideways orientation as shown above in Figure 4. By contrast, on the quintet surface the transition state for hydrogen abstraction is established by an electron shift from σ_{C-H} toward the empty $\sigma^*_{z^2}$ orbital that is aligned along the *z*-axis. Thus, to maximize the $\sigma_{C-H}-\sigma^*_{z^2}$ overlap the ^{5}**TS$_H$** assumes an upright structure, as shown in Figure 4. During the rebound step on the triplet surface, the electron shifts from the singly occupied orbital of the radical, ϕ_C, to the empty $\sigma^*_{z^2}$ orbital of the iron−hydroxo complex. Therefore, the rebound transition state on the triplet surface, ^{3}**TS$_{reb}$**, will assume now an upright orientation, as seen in Figure 5.

In the quintet rebound via ^{5}**TS$_{reb,\beta}$** (Figure 5), the electron of the cyclohexyl radical in the orbital ϕ (Scheme 4) is donated to $\sigma^*_{z^2}$, thereby causing a rather upright geometry with an Fe−O−C angle of 169.0°. The rebound nascent from ^{5}**I**$_\alpha$ involves an electron shift to the δ orbital, and we note that the overlap of ϕ with this orbital is very poor. Therefore, the electron of the cyclohexyl radical in ϕ will be donated to the iron center indirectly via the π^* orbital,[32] thus leading to an Fe−O−C angle of 157.1°, which is smaller than in ^{5}**TS$_{reb,\beta}$** (169.0°).

4.2. Origins of the EF effects during the Reaction of TMC(SR)FeO$^+$ with C$_6$H$_{12}$. These orbital selection rules and their resultant transition state geometries are associated with a change of the dipole moment of the molecular species, and hence, the interaction with the external EF will be both species-selective and spin-state selective as found above in Figure 3b. Figure 6a shows the variation of the dipole moment along the reaction path for the triplet and quintet states. Initially, at the reactants stage, the dipole of **K$_{TMC(SR)}$** is oriented along the FeO axis, from TMC(SR) where the negative pole is to Fe where the positive pole is. Therefore, application of the EF in the $-z$ direction stabilizes the reactants. As soon as the substrate is coordinated to the iron−oxo reagent, in the **RC** complex, there is some charge transfer from the substrate to the FeO, which increases as the reaction progresses. Therefore, the magnitude of the dipole moment in the $+z$ direction will increase along the reaction coordinate, and will lead to a concomitant increase of the stabilization of the molecular system by the external EF. As further seen in Figure 6b, this stabilization is augmented by the induced dipole that is coaligned with the field-free dipole, thus generating a large molecular dipole.

The available stabilization energy (SE) values, or energy change, due to application of EF, is plotted in part c of Figure 6 and is seen to increase with the size of the dipole of the species: the **RC** complex is stabilized slightly compared with the reactants, the **TS$_H$** species even more, and the **TS$_{reb}$** species still more, while the products undergo the largest stabilization. The quintet ^{5}**TS$_H$** and ^{5}**I** species have larger dipole moments than the corresponding triplet state species and are hence more affected by the EF. Thus, the direct relationship between the stabilization energy and the molecular dipole provides the root cause for the results in Figure 3b above, where the EF is seen to lower the energy of all the species relative to the reactants.

The increase of the stabilization of these species is due to two factors, which in turn affect the size of the dipole: (i) increase in the charge transfer from the cyclohexane to the iron−oxo reagent; (ii) changes in geometry. Thus, while the first factor is responsible for the lowering of all the species in energy, the second factor is responsible for the spin-selective effects. Accordingly, since ^{5}**TS$_H$** is upright while ^{3}**TS$_H$** is more sideways, the former has the larger dipole and its stabilization is more significant. The stabilization of both **TS$_H$** species is consistent with the shifting of their geometries to an earlier position along the H-transfer coordinate (Figure 4). During the rebound, the ^{3}**I** intermediate has a sideways orientation (Figure 5), while the corresponding rebound transitions state ^{3}**TS$_{reb}$** is upright and has a larger dipole. This is the reason the rebound barrier on the triplet surface (Figure 3b) drops dramatically in the presence of the EF. The rebound transition states on the quintet surface, ^{5}**TS$_{reb,\alpha(\beta)}$**, are also upright or nearly so, and their large dipole moment causes stabilization and complete elimination of these transition states. Therefore, the external EF improves the efficiency of the rebound process for both spin states by facilitating the electronic rearrangement.

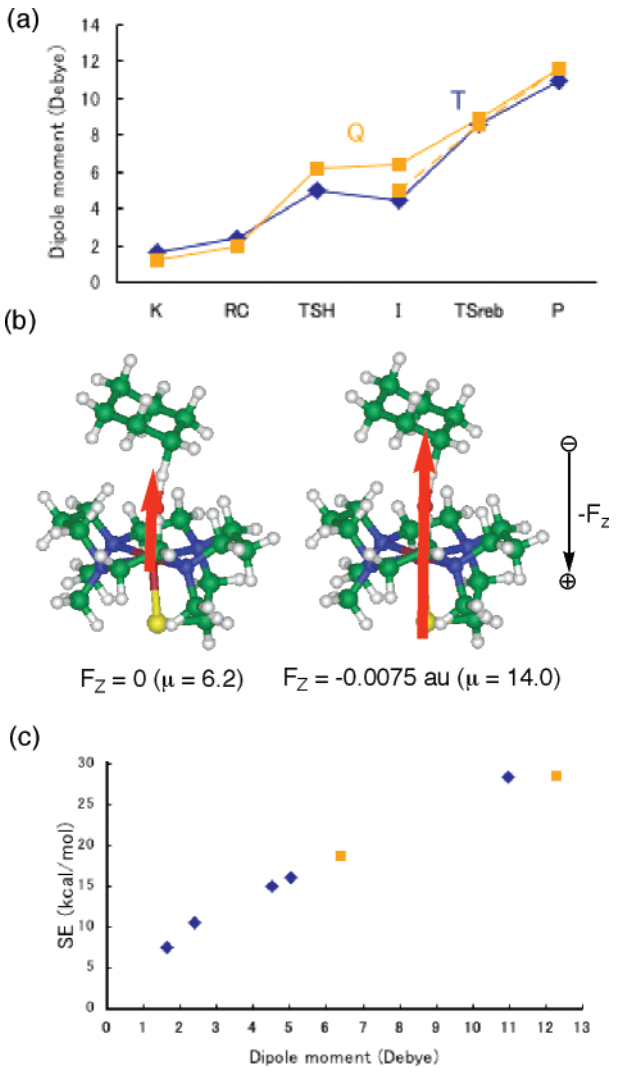

Figure 6. (a) Variation of the dipole moment (μ, in D) along the reaction path for $F = 0$. Blue diamonds are for the triplet state, while orange squares are for the quintet state. The dipole orientation of the free iron−oxo reagent is shown in the plot. The dashed line corresponds to the process from ^{5}**I**$_\beta$ to ^{5}**P**. (b) Directions and magnitudes of the molecular dipole for the ^{5}**TS$_H$** species for $F = 0$ and $F_z = -0.0075$ au. (c) Schematic variation of the stabilization energy (SE taken as positive) by the EF along the reaction path.

(32) By reference to Scheme 6, the electron in ϕ_C is shifted to π^* and, in turn, an electron from the latter orbital is demoted to the δ orbital.

4.3. Directional Selectivity of the EF Effect. As argued above (e.g., Figure 6c), the EF acts upon the molecular system by primarily interacting with the molecular dipole. For the systems studied here, the molecular dipole is oriented in the direction from the axial ligand L to the Fe−O−H−R moiety (Figure 6b), and therefore, it is natural to find that the orientation of the EF in the opposite direction (Figure 6b) exerts the most beneficial and largest effect on the energy profile. Furthermore, on the basis of the evolution of the electronic structure along the reaction path in Scheme 6, there is *an electronic flow during oxidation from the substrate RH down to the iron−oxo reagent*, exactly in the preferred direction of the EF polarity. We may therefore conclude that the orientation of the EF in the direction of the electron flow during the reaction dramatically changes the reaction energy profiles for C−H hydroxylation by a nonheme iron−oxo complex and can lead to high reactivity and higher stereoselectivity with appropriately labeled substrates. Since chemical reactions are essentially electron reorganization processes, these EF effects are expected to be general. A simple selection rule can thus be derived: *an external EF will induce higher reactivity and selectivity in a reaction if it is oriented along the "reaction axis" in a manner that enhances the electron flow needed for the completion of the reaction.*

5. Conclusion

This study shows that an external EF acts as an accessory catalyst. If the EF is oriented in the direction of the electron flow, it will dramatically change the mechanism and the energy landscape of an oxidation reaction by a nonheme iron−oxo catalyst. When the iron−oxo reagent and substrate constitute a good electron acceptor/donor pair, the application on an EF in will change the mechanism from H-abstraction and radical formation to an electron-transfer mechanism and a cabocation formation. However, when the iron−oxo is not a powerful acceptor as is the case in TMC(SR)FeO^{2+} and the substrate a poor donor like cyclohexane, the EF will not change the mechanism but will improve the rates of both H-abstraction and rebound step and will, therefore, lead to high reactivity and stereospecificity and lower yield of side products.

Since chemical reactions are essentially electron reorganization processes, these EF effects are expected to be general. Implementation of these ideas may not be technically simple and will require a clever experimental design to orient the iron−oxo reagent. This can potentially be achieved by adding small hydrocarbon chains with appropriate substituents that can lead to adsorption on surfaces, e.g., gold surface, or on an AFM/STM tips, an electrode, etc. In such an event the EF effects will be maximized. If however, the EF will be applied to a reaction in solution, the free rotation of the molecules will average the EF and will lead to smaller effects.

Acknowledgment. S.S. acknowledges a DIP grant (DIP-G7.1). H.H. is a JSPS postdoctoral fellow for research abroad. H.C. thanks the Golda Meir Fund. M.A.C. is supported by the Department of Education and Universities of the Autonomous Government of Catalonia.

Supporting Information Available: Additional figures and tables, methods, and complete ref 23. This material is available free of charge via the Internet at http://pubs.acs.org.

JA070903T